ACS APPLIED MATERIALS & INTERFACES

Research Article

www.acsami.org

Polymer Sol–Gel Composite Inverse Opal Structures

Xiaoran Zhang and G. J. Blanchard*

Department of Chemistry, Michigan State University, 578 S. Shaw Lane, East Lansing, Michigan 48824, United States

Supporting Information

ABSTRACT: We report on the formation of composite inverse opal structures where the matrix used to form the inverse opal contains both silica, formed using sol–gel chemistry, and poly(ethylene glycol), PEG. We find that the morphology of the inverse opal structure depends on both the amount of PEG incorporated into the matrix and its molecular weight. The extent of organization in the inverse opal structure, which is characterized by scanning electron microscopy and optical reflectance data, is mediated by the chemical bonding interactions between the silica and PEG constituents in the hybrid matrix. Both polymer chain terminus Si–O–C bonding and hydrogen bonding between the polymer backbone oxygens and silanol functionalities can contribute, with the polymer mediating the extent to which Si–O–Si bonds can form within the silica regions of the matrix due to hydrogen-bonding interactions.

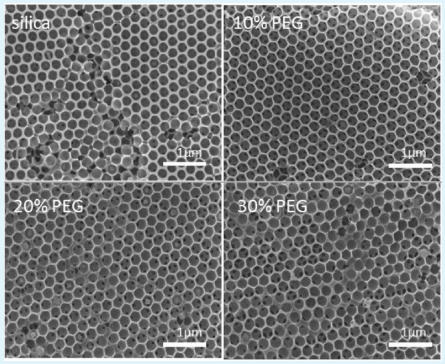

KEYWORDS: *inverse opal, silica sol–gel, PEG, hybrid matrix, three-dimensionally ordered macroporous (3DOM)*

INTRODUCTION

Organic–inorganic hybrid materials have been studied for decades and applied to optical, electronic, and mechanical technologies.[1] The goal of creating such hybrid composite materials is to combine the most useful properties of each constituent material to produce materials with superior performance for specific applications.[2] Sol–gel chemistry is useful in the construction of some composite materials because of its low-temperature processing and its ability to combine with functionalized organic species, including polymers. The broad range of sol–gel chemistry available allows for the versatile design of hybrid inorganic/organic materials containing metal alkoxides and alkoxysilanes,[3] providing broad control over the properties of the resulting materials.[4] In any such work, the characteristic length scale of the compositional heterogeneity is critically important, as is the chemical nature of the interface between different compositional regions.[5] For this reason, it is necessary to evaluate such systems experimentally, especially when they are used in the formation of intricate structures such as inverse opals.

We are interested in inverse opal, also called three-dimensionally ordered macroporous (3DOM) structures because of their ability to combine several chemical and physical properties that are useful in catalyst support applications. Specifically, inverse opals are moderately high surface area, they can form flow-through structures with controllable void volumes and pore diameters, and the surface reactivity can allow for the chemical attachment of selected catalytic species. In addition, the close-packed ordered porous structure with a pore size of a few nanometers to micrometers endows 3DOM materials with useful optical and photonic crystal properties.[6] This material structure can be utilized in optical information processing and storage devices, sensors, fuel cell electrodes, catalyst supports, and bioactive materials.[7−9] The construction of inverse opals is well established, and there is extensive literature extant on sol–gel chemistry.[10,11] When using sol–gel chemistry to create inverse opal structures, it is frequently challenging to create macroscopic regions that are free of defects and cracks. Such features limit the utility of the resulting structure because they provide channels that can bypass functionalized regions of the structure. A major reason for the formation of defects in inverse opal structures is that the support on which the inverse opal is formed does not undergo dimensional change as the sol cures and contracts, and the resulting stresses in the inverse opal structure are alleviated by cracking and defect formation. One goal of our work is to create inverse opal structures that can serve as flow-through catalyst supports and that do not exhibit high defect densities and/or cracks.

In an effort to create inverse opal structures on a porous alumina support that are characterized by a lower defect density than those formed using silica sol–gel chemistry alone, we have explored the use of poly(ethylene glycol), PEG, as a matrix additive. Our data reveal a reduction in visible defect and crack density with the addition of PEG, and the extent of structural improvement is found to depend on the amount of PEG and its molecular weight. The primary focus of this work is on understanding the dependence of the hybrid matrix composition on the quality of the inverse opal structure formed.

Received: August 22, 2014
Accepted: March 3, 2015
Published: March 3, 2015

DOI: 10.1021/acsami.5b00656
ACS Appl. Mater. Interfaces 2015, 7, 6054–6061

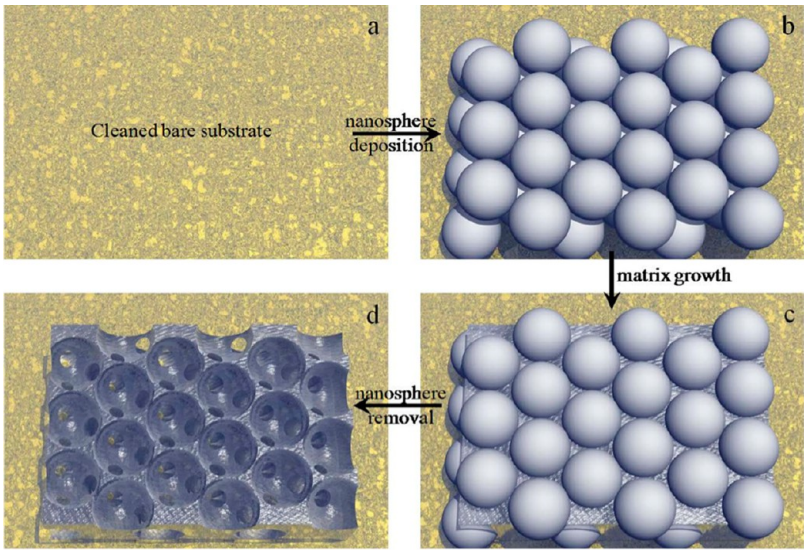

Figure 1. Schematic of the construction of an inverse opal structure. In this work, (a) the support is a porous alumina membrane. (b) The nanospheres are polystyrene and template self-assemblies. (c) The matrix material is formed using silica sol–gel chemistry, with or without added PEG. (d) The nanosphere template is removed by toluene.

EXPERIMENTAL METHODS

Experimental Materials. Styrene (C_8H_8, ≥99%, Sigma-Aldrich), potassium persulfate ($K_2S_2O_8$), sodium *p*-styrenesulfonate ($C_8H_7SO_3Na$), potassium bicarbonate ($KHCO_3$), sodium hydroxide solution (1 wt % NaOH in water), 2,2-azobis(isobutyronitrile) (AIBN, 98%, Aldrich), tetraethylorthosilicate (TEOS, ≥99%, Aldrich), ethanol (anhydrous), hydrochloric acid (12 M, Columbus Chemical Industries), poly(ethylene glycol) methyl ether (average M_n = 750 g/mol, Aldrich) poly(ethylene glycol) (BioUltra, 2000 g/mol, Sigma), poly(ethylene glycol) (10 000 g/mol, Fluka), toluene (≥99.5%, Mallinckrodt), and water (Milli-Q), were used as received, without further purification. Whatman Anodisc filter membranes (porous alumina substrate, d = 13 mm, pore size 200 nm, unsupported) were used as the inverse opal supports.

Nanoporous Silica Structure Fabrication. Polystyrene colloidal spheres with an average diameter of 290 nm were synthesized by an emulsion polymerization method.[12] Styrene was washed using a 1% sodium hydroxide solution and distilled prior to use to remove the stabilizer. Distilled styrene monomer was added into 100 mL of deionized (DI) water and heated to 72 °C. Potassium bicarbonate and sodium *p*-styrenesulfonate were dissolved in DI water, preheated to 72 °C, and transferred to the styrene-containing solution. The reaction is initiated by AIBN and refluxed at 72 °C for 28 h. The resulting solution was evaporated to dryness using a rotary evaporator.

Colloidal crystal templates were made by the evaporation method.[13,14] Porous alumina substrates were placed vertically into 0.25 wt % polystyrene solution. After evaporation at 65 °C for 10 h, close-packed colloidal crystal templates were formed on the porous alumina substrates as uniform films that exhibited strong diffraction of light.

The silica–PEG hybrid matrix was prepared using sol–gel chemistry.[15,16] Silica sol–gel solutions were made for deposition with a range of PEG loadings (0, 10, 20, and 30 wt %, each with M_n = 2000 g/mol PEG) and with a range of PEG molecular weights (750, 2000, and 10 000 g/mol, each at 10 wt %). After dissolution of PEG in ethanol (7.5 mL), precursor solutions were obtained by mixing TEOS (1.15 mL), Milli-Q water (0.9 mL), 12 M HCl (65 μL), and PEG for 1 h. The polystyrene (PS) nanosphere template on a porous alumina substrate (PAS), PS/PAS for short, was supported on a glass frit and a vacuum is applied (water aspirator).[17] The sol–gel solution is added dropwise on the PS/PAS structure so that the sol–gel can fill the interstitial spaces within the nanosphere array. The resulting assembly is dried at 50 °C for 48 h and then placed in toluene for 24 h to remove the polystyrene nanospheres.

Transmission Electron Microscopy (TEM). TEM images were obtained using an ultra-high-resolution JEOL 2200FS transmission electron microscope located in the Center for Advanced Microscopy at Michigan State University (MSU). Acceleration voltage was 200 kV.

Scanning Electron Microscopy (SEM). Samples were sputter-coated with Os for 20 s and SEM images were obtained using an ultra-high-resolution JEOL 7500F scanning electron microscope housed in the Center of Advanced Microscopy at Michigan State University. Acceleration voltage was 5 kV for all images.

Attenuated Total Reflectance Infrared Spectroscopy (ATR-IR). ATR-IR spectra were obtained using a Perkin-Elmer Spectrum One FT-IR spectrometer over the spectral range of 650 to 1500 cm^{-1}. Spectral resolution for all measurements was 4 cm^{-1} and each spectrum was the result of 1024 acquisitions.

Ultraviolet–Visible (UV–Vis) Spectroscopy. UV–visible reflectance spectra were obtained using a Perkin-Elmer Lambda 35 UV/visible spectrometer. Data were acquired from 200 to 1000 nm, with a spectral resolution of 1 nm.

Thermogravimetric Analysis (TGA). TGA measurements were performed using a TA Q500 instrument (TA Instruments) in high-resolution mode with a thermal ramp rate of 25 °C/min between room temperature and 750 °C, under dry nitrogen. For these measurements, samples were measured before and after thermal curing at 200 °C for 2 h.

Dynamic Light Scattering (DLS). The size of the polystyrene spheres was measured using Malvern Zetasizer Nano ZS. The spheres were suspended in an aqueous solution for analysis.

RESULTS AND DISCUSSION

We are interested in understanding the effect of adding PEG to a silica sol–gel matrix for the purpose of making high-quality inverse opal structures, schematized in Figure 1. The properties of the inverse opal structures as a function of PEG molecular weight and loading in the sol are of primary interest but issues other than the composition of the hybrid matrix can play a role in the quality of the resulting inverse opal structures.

A key factor in the growth of high-quality inverse opal structures is the monodispersity and surface properties of the polystyrene nanospheres used. Polystyrene colloidal spheres with an average size of 290 ± 30 nm were prepared using emulsifier-free emulsion polymerization (Supporting Information).[12] From these nanospheres the template was self-

DOI: 10.1021/acsami.5b00656
ACS Appl. Mater. Interfaces 2015, 7, 6054–6061

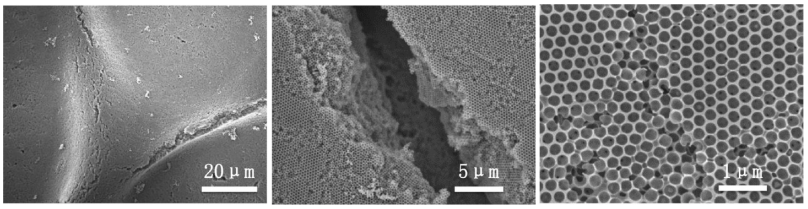

Figure 2. SEM images of an inverse opal formed using silica sol–gel chemistry with no added PEG. The magnifications are (left to right) 1200×, 5000×, and 23 000×, with corresponding scale bars indicating 20, 5, and 1 μm.

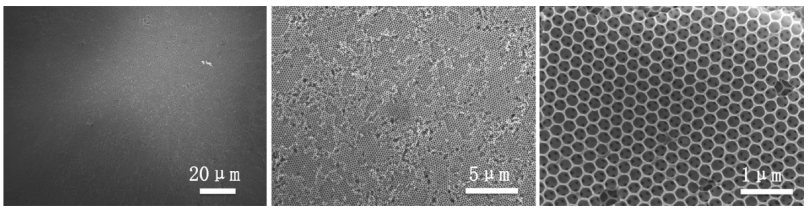

Figure 3. SEM images of an inverse opal formed using silica sol–gel chemistry with 10 wt % PEG (M_n = 750 g/mol). The magnifications are (left to right) 800×, 4000×, and 23 000×, with corresponding scale bars indicating 20, 5, and 1 μm.

assembled by evaporation (Figure S2).[13] The sol–gel precursor mixture was aspirated into the nanosphere template and the sol–gel reaction was allowed to proceed, resulting in the formation of a silica matrix. Once the matrix was formed, the polystyrene nanospheres were removed by dissolution and a 3D nanoporous inverse opal structure resulted.

Effect of PEG Loading on the Hybrid Matrix. To investigate the effect of PEG in silica–PEG hybrid materials, the nanoporous matrixes have been fabricated using silica precursor only and silica precursor mixed with 10% PEG (M_n = 2000 g/mol). For the silica-only matrix (Figure 2), significant cracks were formed in the structure and these were associated with matrix curing and consequent contraction. With the addition of PEG, the uniformity of the nanoporous matrix improves significantly, as can be seen in Figure 3. In the SiO_2–PEG composite system, any covalent chemical interaction between the polymer and silica network must be through Si–O–C covalent bonds at the polymer chain termini, and hydrogen bonding may also occur between ether oxygens in the polymer backbone and free silanol groups in the silica matrix.[18] We note that the propensity for the Si–O–C bonds to form will differ for the PEG of M_n = 750 g/mol because it is present as the methyl ether, while the higher molecular weight PEGs exist in the hydroxyl-terminated form. These interactions allow the silica sol–gel to produce a matrix with fewer defects while retaining properties of the polymer, such as elasticity and mechanical robustness.[19] The central question is why the addition of PEG to the silica sol–gel mitigates the formation of defect structures. It is likely that the presence of PEG occupies a sufficient number of silanol groups that the silica matrix does not "cure" (i.e., form Si–O–Si bonds) fully, thereby reducing contraction in the formed material and leading to increased elasticity. We will explore this possibility using FTIR and thermogravimetric analysis (vide infra).

To evaluate the nature of the matrix enhancement produced by the addition of PEG to the silica sol–gel, it is important to consider both the chemical structure and the thermal properties of the resulting hybrid material. We consider first the effect of PEG loading in hybrid, sol–gel solutions. We have made hybrid systems for deposition on a nanoparticle scaffold with PEG loadings of 0, 10, 20, and 30 wt % (M_n = 2000 g/mol). Although the addition of PEG improves the quality of the matrix, increasing the polymer loading results in the appearance of defects on its surface, as is seen by comparing Figures 2 and 3.

At this point it is important to consider how the characterization of defects can be organized for such systems. Clearly, defect structures exist on several different length scales and to speak simply of a defect density is a misleading oversimplification. For this reason we identify five different types of defects. These are cracks, void defects, pore defects, hole defects, and wall defects. Cracks are breaks in the inverse opal structure and can range from macroscopic (Figure 2, center) to more localized in extent (Figure 2, right). For the inverse opal structures we report here, the expected void diameters are from 0.23 to 0.26 μm. Voids are considered to be defective if their diameters are less than 0.20 μm or greater than 0.29 μm ("V", Figure 4a). In certain instances, void defects are

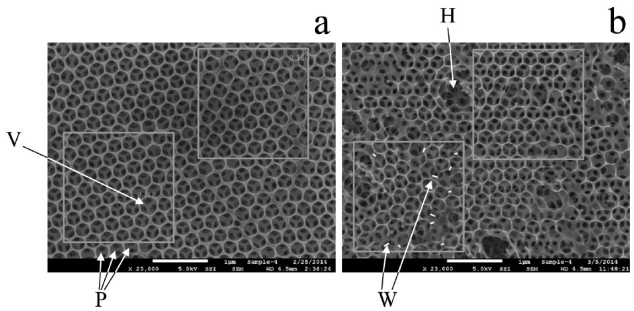

Figure 4. Types of defects characterized for inverse opal structures. (a) An inverse opal structure characterized primarily by types V and P defects. (b) An inverse opal structure that contains types H and W defects in addition to types V and P defects. The boxed areas are representative selected areas (2 × 2 μm) in which defect-type densities were counted.

of sufficient size to encompass more than one void, causing disruption of intervoid walls both in-plane and between planes of the inverse opal structure ("H", Figure 4b). Such defects are termed hole defects. In a regular inverse opal structure based on a hexagonal close-packed nanosphere multilayer structure, there are three pores that can be seen in each void. These pores correspond to the three point contacts made by each

DOI: 10.1021/acsami.5b00656
ACS Appl. Mater. Interfaces 2015, 7, 6054–6061

Table 1. Densities of Different Types of Defects as a Function of PEG Loading[a]

number/μm^2	cracks	void defects	pore defects	hole defects	wall defects
0 wt %*	0.17.0 ± 0.2	0.8 ± 0.7	13.5 ± 2.5	0	1.5 ± 0.3
10 wt %	0	1.2 ± 1.3	3.9 ± 1.7	0	3.0 ± 1.9
20 wt %	0	0.4 ± 0.3	14.5 ± 1.2	0	2.5 ± 0.7
30 wt %	0	0.6 ± 0.4	14.0 ± 1.7	0	4.2 ± 2.1

[a]Uncertainties are reported as $\pm 1\sigma$ for six individual determinations.

nanosphere in the scaffold with its underlayer, and interlayer dislocations or misregistrations cause disruptions in this pattern. When a void has more or less than three pores, it is characterized as a pore defect ("P", Figures 4a,b). The fifth type of defect is termed a wall defect ("W", Figures 4a,b). The normal thickness of the walls between voids is less than 0.045 μm and wall thickness greater than 0.05 μm is considered to be defective. We have not placed a lower bound on this type of defect because the partial or complete absence of a wall leads to a hole-type defect.

Defect densities were determined by counting the number of defects of each type per unit area (Table 1). Such a reporting of defect density relies on the measurement of multiple samples to provide reasonable accuracy. The structures we report are reproducible in terms of defect densities for each composition, despite the uniqueness of each individual structure.

The addition of PEG to the sol–gel significantly decreases the appearance of cracks in the inverse opal structure and depending on the density of pore defects. The most regular inverse opal structure, in terms of P-type defects, appears for 10 wt % PEG, with substantial degradation in the regularity of the structure for higher polymer loadings. The pore defect density increases with that of wall defects. It appears (Figure 5) that the

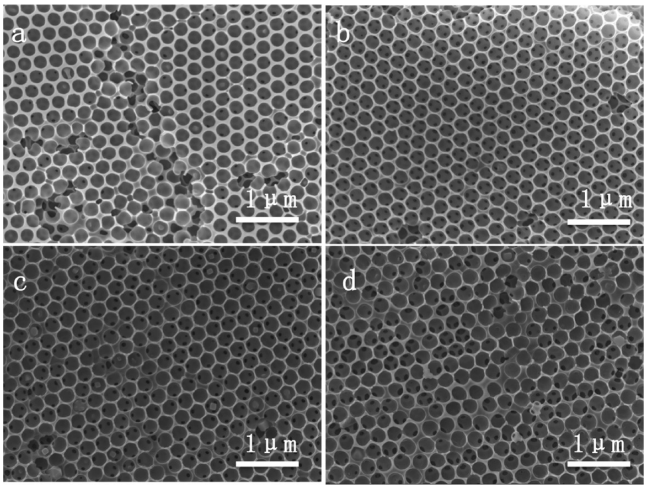

Figure 5. SEM images of inverse opal structures resulting from the addition of PEG (M_n = 2000 g/mol) to the sol used in matrix formation. (a) 0 wt % PEG, (b) 10 wt % PEG, (c) 20 wt % PEG, and (d) 30 wt % PEG.

wall thickness of the inverse opal structures depends on the polymer loading and we understand this in the context of PEG altering the surface tension of the sol–gel precursor solution, a factor which influences the size of the pores formed.

As noted above, the interactions between PEG and the silica matrix are covalent (chain-end) bonds and hydrogen bonds between the polymer ether oxygens and free silanol groups in the silica matrix. PEG is a linear polymer and morphological effects relating to the molecular weight of the polymer represent a balance between H-bonding and terminal group effects. Because of the relative contribution of each interaction, we assert that it is changes in the extent of H-bonding interactions that are responsible for the observed changes in morphology. Specifically, the presence of the polymer in the hybrid matrix serves to relax strain imposed on the silica matrix by the formation of Si–O–Si bonds. If the polymer content of the material is too high, however, it can limit the extent of Si–O–Si bond formation to the point where the integrity of the matrix is compromised. While it is not possible to quantify this effect because of the complexity and molecular scale disorder in the hybrid matrix, we attempt to characterize this balance phenomenologically through FTIR and thermogravimetric means.

One issue that is useful to consider is the relative size of the species and features in the matrix. The nanospheres used to form the scaffold structures for the formation of the matrix are ca. 290 nm diameter. The radius of gyration for PEG provides a qualitative measure of the expected spatial extent of the PEG-containing features in the hybrid matrix. The hydrodynamic radius of PEG in water has been determined to be ca. 4 nm for M_n = 20 000.[20] Given that the PEG polymers we use are all lower molecular weight, the radius of gyration will be less than 4 nm, and in any event this length scale is much shorter than that of the physical features that characterize the inverse opal structure. Thus, the defects seen in the hybrid matrix structure for higher molecular weight polymers cannot be attributed directly to the increase in polymer molecular weight. Rather, we believe it is the extent of matrix "curing" that is achievable for the different polymer molecular weights that is responsible for the differences we observe. We turn next to consideration of the molecular-scale organization of the hybrid matrix.

ATR-FTIR. One of the more sensitive structural probes for the hybrid matrixes considered here is vibrational spectroscopy. Attenuated total reflectance (ATR) infrared spectra of the silica–PEG hybrid matrix, as an inverse opal structure, are shown in Figure 6 as a function of PEG loading. The spectra are for hybrid matrixes containing 0, 10, 20, and 30 wt % PEG (M_n = 2000 g/mol), as indicated. Also shown is the ATR-FTIR spectrum of PEG (top). On the basis of the spectra of PEG and of silica, we can assign the Si–O–Si asymmetric stretching mode at 1067 cm^{-1} and at 1108 cm^{-1} (shoulder), and the C–O–C symmetric stretching band at 1097 cm^{-1}. When the PEG loading is increased, the C–O–C peak shifts from 1030 to 1100 cm^{-1}, consistent with the introduction of PEG into the silica sol–gel system. The CH_2 bending and wagging modes appear at 841, 1146, 1279, 1341, and 1467 cm^{-1} and the CH_2 asymmetric stretch at 2882 cm^{-1}.[15,21] The peak at 950 cm^{-1} is assigned to the silanol Si–O symmetric stretch and the peak at 958 cm^{-1} is $-CH_2$ rocking.[15,21] The absence of a peak in the vicinity of 3500 cm^{-1} indicates that there are few residual silanol functionalities that are not involved in H-bonding. What is important to note are the changes associated with the

DOI: 10.1021/acsami.5b00656
ACS Appl. Mater. Interfaces 2015, 7, 6054–6061

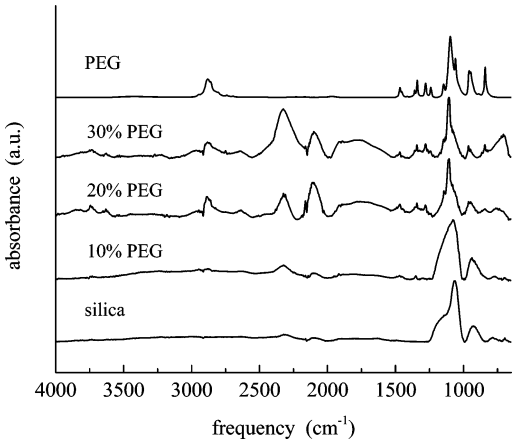

Figure 6. Infrared spectra of (bottom to top) 0, 10, 20, and 30 wt % PEG (M_n = 2000 g/mol) in silica–PEG inverse opal matrix, and pure PEG (M_n = 2000 g/mol).

addition of PEG to the hybrid matrix. We focus primarily on the CH stretching region because that is the most information-rich in terms of the polymer–silica interactions. For both silica (only) and PEG (only), there are no significant spectral features in the vicinity of 3700 cm^{-1} and we understand this in terms of the comparative absence of silanol groups for silica and a small number of terminal functionalities for PEG. For 20 and 30 wt % PEG in silica, there are measurable bands in the 3700 cm^{-1} region, indicating the presence of unassociated silanol functionality in the silica matrix.[22] For 10 wt % PEG, there is relatively little feature in this region, suggesting much less unassociated silanol functionality. This finding is consistent with only modest structural disruption being imposed by 10 wt % PEG, but higher PEG loadings giving rise to structural disruption that is more extensive, presumably by preventing Si–O–Si linkages from being formed to their fullest extent. We assert that it is the inability to form Si–O–Si linkages extensively that is correlated with the increase in structural defects in the inverse opal structures. Taken collectively, the ATR-FTIR data show that the PEG incorporates into the sol–gel matrix and that the organization of both the polymer and the silica matrix depends on the amount of polymer present.

Thermogravimetric analysis (TGA) analysis can be useful in evaluating the structural integrity of the hybrid matrix. Approximately 10 mg of the inverse opal on the porous alumina substrate was heated to 750 °C in an alumina pan.[23] Because the inverse opal samples were bound to the porous alumina substrate, it is not possible to know the mass of each component, and the weight loss curves were normalized to the same baseline to compare trends in the data (Figures 7 and 8). The absolute weight loss is not the focus of these results. The TGA measurements provide information on the relative thermal stability of the silica–PEG inverse opal matrix as a function of matrix composition. There are clear trends in the TGA data.

The first feature of note is that the thermal profile for PEG is a clean stepwise change at ~380 °C, indicative of the decomposition of the polymer backbone. For the silica matrix, however, there is a more gradual change with increasing temperature. We attribute this loss to the progressive dehydration of silanol groups, and the formation of Si–O–Si linkages where it is structurally feasible. It is worth noting that the addition of PEG increases the thermal stability of the silica

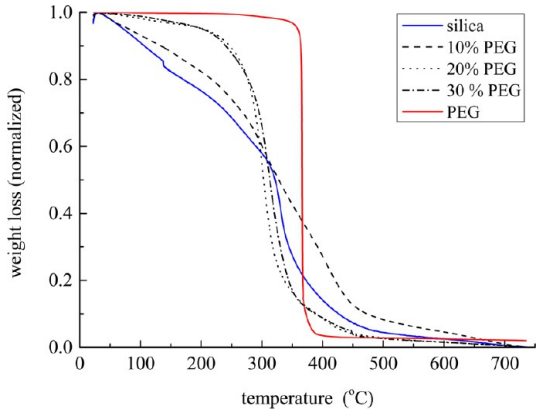

Figure 7. Thermogravimetric analysis of silica–PEG inverse opal structures with PEG loadings of 0, 10, 20, and 30 wt % and pure PEG, without curing at 200 °C for 2 h.

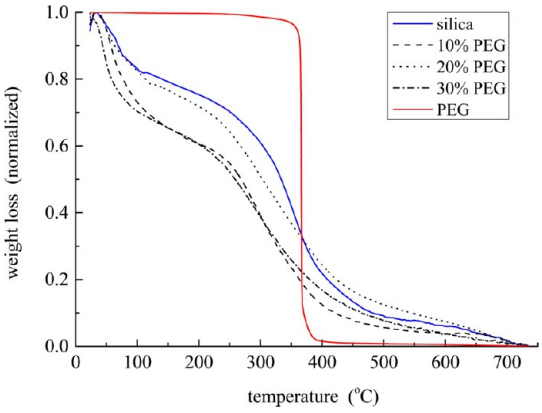

Figure 8. Thermogravimetric analysis of silica–PEG inverse opal structures with PEG loadings of 0, 10, 20, and 30 wt % and pure PEG, after initial curing at 200 °C for 2 h.

sol–gel prior to curing, and for temperatures below ca. 300 °C. This result is different with the traditional organic–inorganic hybrids, which exhibit increased thermal stability with increasing inorganic component content. A likely explanation for our results is incomplete curing of the silica sol–gel. The samples were cured for 2 h at 200 °C and TGA trace changes were observed. The network might experience further condensation and form larger scale networks. During further curing at 200 °C, the reaction of "dangling" bonds to form the bridging bonds is possible.[24] The thermal decomposition curves for silica and the hybrid matrix with 10 wt % PEG are similar, and both are different than the (similar) curves for 20 and 30 wt %. We understand these differences in terms of the extent of structural disruption within the hybrid matrix imposed by the presence of PEG. What is somewhat surprising is the similarity of the TGA data for the silica matrix and the hybrid matrix with 10 wt % PEG. These two matrixes are characterized by the greatest difference in macroscopic morphology while retaining the greatest similarity in terms of thermal properties. This is a matter that remains under investigation. The overall trend in the TGA data as a function of matrix composition is that the thermal properties progress qualitatively from being silica-like to being PEG-like, but the trend is not a smooth function of matrix composition.

Effect of PEG Molecular Weight on the Hybrid Matrix. In addition to the effect of matrix composition, it is also

DOI: 10.1021/acsami.5b00656
ACS Appl. Mater. Interfaces 2015, 7, 6054–6061

Table 2. Defect Densities as a Function of PEG Molecular Weight (10 wt % Loading)[a]

number/μm^2	cracks	void defects	pore defects	hole defects	wall defects
M_n = 750 g/mol[b]	0	0.08 ± 0.13	2.16 ± 1.30	0	0.75 ± 0.89
M_n = 2000 g/mol	0	1.17 ± 1.33	3.92 ± 1.71	0	2.96 ± 1.91
M_n = 10 000 g/mol	0	0	2.42 ± 0.82	1.29 ± 0.43	1.29 ± 0.9

[a]Uncertainties are reported as ±1σ for six individual determinations. [b]PEG is methoxy-terminated.

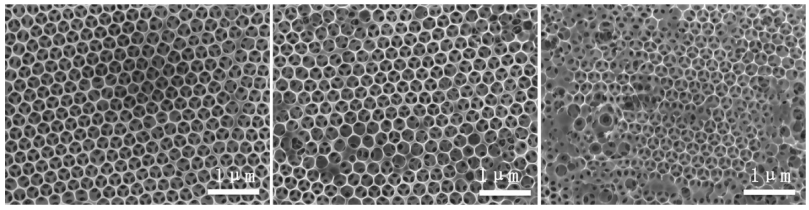

Figure 9. SEM images of inverse opal structure made with 10 wt % PEG of different molecular weights (from left to right): 750, 2000, and 10 000 g/mol.

important to consider the effect of PEG molecular weight on the morphology and properties of the hybrid matrix. To evaluate the PEG molecular weight dependence, we used PEG with molecular weights of 750, 2000, and 10 000 g/mol, each at 10 wt % loading in the sol–gel solution. It is shown in Table 2 that no cracks appear with PEG of any molecular weight loading in the matrix. Increasing the molecular weight of PEG in the hybrid matrix influences the resulting matrix structure, as shown in Figure 9. The number of void, wall, and pore defects for 10 000 g/mol PEG loading is lower than is seen for PEG of 2000 g/mol, although this is not clear based on casual inspection. The reason for this is that the larger hole area takes the space that would have been occupied by regular voids, and the actual number of void, wall, and pore defects that result from this vacancy are not counted. This finding does not mean that the highest molecular weight PEG necessarily minimizes the defect density in these materials. Rather, we find that once the molecular weight of the PEG increases to 10 000 g/mol, the walls between voids cannot connect consistently and relatively large holes are formed that are sufficiently deep to access lower layers of the structure. For these systems, hole defects become a critical issue that affects the utility of these materials.

We understand the effect of molecular weight in the same context as that of the mass loading. The only expected difference between these two variables is the ratio of end group (Si–O–C) bonds to silanol H-bonds, but the effect of adding more polymer to the matrix (i.e., increasing the number of H-bonds between silanol groups and the polymer backbone) will be the same, and this is found to be the case experimentally.

While it is clear from the SEM micrographs that the organization of the inverse opal structures depends on the composition of the hybrid matrix, attempting to quantitate such organization poses a challenge. Three-dimensional, periodic micro-/nanostructured materials such as inverse opals diffract photons from the lattice of dielectric planes. When the refractive index is large enough, a complete photonic band gap is formed in which Bragg diffraction inhibits a range of wavelengths from propagating through the photonic crystal. This condition can result in the localization of photons and the bands are manifested as brightly colored reflections and an optical filtering effect.[25,26] The optical properties of these materials are influenced by their structural parameters; specifically, the topology, symmetry, defect density, and refractive index contrast inside the photonic crystal determine its optical properties.[26] We can assess the extent of structural organization and defect density by examining the reflective properties of the samples.[27] Through the use of an integrating sphere reflectance accessory to a UV–visible spectrometer, reflectance measurements of opaque solids or powders, and total transmittance scans of translucent films and scattering creams can be recorded. The data presented in Figure 10 show

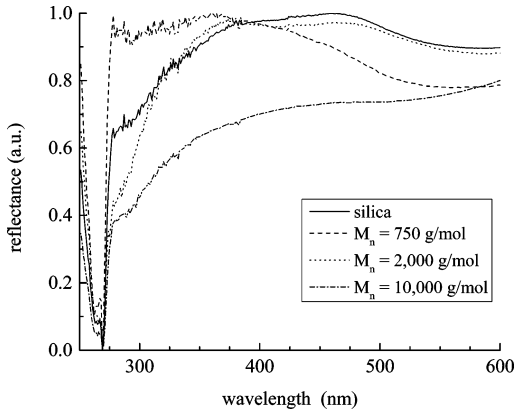

Figure 10. Normalized UV–visible reflectance spectra of inverse opal structures with PEG of M_n = 750, 2000, and 10 000 g/mol. Data were acquired using an integrating sphere.

the UV–visible reflectance spectrum of inverse opal structures containing PEG with molecular weights of 750, 2000, and 10 000 g/mol. The highest contrast peak (ca. 270 nm) is observed for the inverse opal made with PEG of M_n = 750 g/mol. Increasing the molecular weight of PEG produces a peak, with wavelength consonant with the diameter of the void spaces (ca. 290 nm), that is characterized by broad shoulders, consistent with the existence of larger size scale void regions, or defects. It is important to note that the data for the hybrid matrix containing 10 wt % PEG of M_n = 750 g/mol is characterized by a band with a much less prominent shoulder than that seen for the inverse opal structure made using silica sol–gel only.

We attribute the morphology differences of nanoporous structure correlation with the molecular weight to the microscale phase separation. Studies on the silica–PEG hybrid by Jung et al.[19] (in noninverse opal structural format) indicate that such differences are considered to be the result of

DOI: 10.1021/acsami.5b00656
ACS Appl. Mater. Interfaces 2015, 7, 6054–6061

microscale phase separation related to the volume of trapped PEG. Takahashi et al.'s results[28] showed the characteristic length scale of phase separation depends strongly on the amount of polymer, the molecular weight of the polymer, the solvent composition, and the pH. The phase separation that occurs in the silica−PEG sol−gel clearly influences the morphology of resulting inverse opal structure, and the critical H-bonding interactions between the polymer and the silica regions of the matrix are the chemical means by which these separated nanodomains interact. Phase separation mechanisms of silica−PEG/PEO hybrid bulk materials (in noninverse opal strucutural format) has been studied since 1990s by Surviet et al.[29] and Wilkes and co-worker.[30] For shorter polymer chains, like PEG 750, the chance of being encapsulated or forming a mixed phase with condensed TEOS is higher than it is for longer polymer chains. For a longer chain such as PEG 10 000, the formation of an oligomer-rich phase and condensed TEOS clusters is more likely. Therefore, compositional heterogeneity may be seen more readily at the surface of the matrix formed with higher molecular weight PEG.[30]

ATR infrared spectra of the silica−PEG inverse opal structures were also studied as a function of PEG molecular weight (Figure 11). Increasing polymer loading and molecular weight both appear to have a structurally perturbative effect on these composite materials. The observed bands (a composite of silica and PEG bands in the ca. 1000−1200 cm^{-1} region) undergo a shift to higher frequency with the increasing PEG molecular weight. In analogy with the data shown in Figure 6, the peaks at 1180, 1276, 1345, and 2900 cm^{-1} confirm the presence of PEG. While these data do not address the issue of spatial heterogeneity directly, they provide evidence that there is strong interaction between the two phases, as would be expected based on the SEM data on these systems.

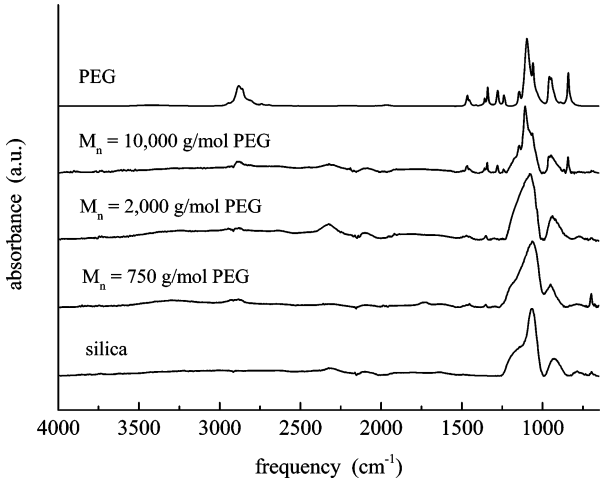

Figure 11. ATR spectra of 10 wt % PEG with M_n = 750, 2000, and 10 000 g/mol and pure PEG (M_n = 2000 g/mol), respectively, from the bottom to top.

CONCLUSION

Traditional silica sol−gel inverse opal structures form significant cracks and defects during the curing process due to shrinkage of the matrix. Addition of poly(ethylene glycol) to the silica sol−gel mitigates cracking and allows for the formation of a matrix containing comparatively few defects. Five kinds of defect density were investigated quantitatively. The morphology of the hybrid matrix depends on the amount of PEG added and its molecular weight. Increases in polymer loading beyond 10 wt % or the use of higher molecular weight PEG leads to structural disruption of the inverse opal matrix structure. The conformation of interactions between the polymer and silica network components mediates the morphological and thermal properties of the hybrid matrix material.

This work points the way to the use of other more structurally versatile polymers as potential components in hybrid matrix structures. In addition to the matrix components, there are also structural and physical issues to be addressed, including more thorough characterization of the polymer−matrix interactions and the interactions between the matrix and its support. These issues will be important for further improvements in the construction of low-defect hybrid matrix inverse opal materials.

ASSOCIATED CONTENT

Supporting Information

TEM image of polystyrene nanospheres and nanosphere assembly. This material is available free of charge via the Internet at http://pubs.acs.org.

AUTHOR INFORMATION

Corresponding Author

*E-mail: blanchard@chemistry.msu.edu. Tel.: +011 517 355 9715.

Notes

The authors declare no competing financial interest.

ACKNOWLEDGMENTS

We are grateful to the Donors of the ACS Petroleum Research Fund for their support of this work through Grant 52692-ND6 and to the MSU Microscopy Facility for their assistance with the acquisition of the images reported here.

REFERENCES

(1) Judeinstein, P.; Sanchez, C. Hybrid Organic-Inorganic Materials: A Land of Multidisciplinarity. *J. Mater. Chem.* **1996**, *6*, 511−525.
(2) Schottner, G. Hybrid Sol-Gel-Derived Polymers: Applications of Multifunctional Materials. *Chem. Mater.* **2001**, *13*, 3422−3435.
(3) Mammeri, F.; Le Bourhis, E.; Rozes, L.; Sanchez, C. Mechanical Properties of Hybrid Organic-Inorganic Materials. *J. Mater. Chem.* **2005**, *15*, 3787−3811.
(4) Pierre, A.; Rigacci, A. In *Aerogels Handbook*; Aegerter, M. A., Leventis, N., Koebel, M. M., Eds.; Springer: New York, 2011; pp 21−45.
(5) Shea, K. J.; Loy, D. A. Bridged Polysilsesquioxanes. Molecular-Engineered Hybrid Organic-Inorganic Materials. *Chem. Mater.* **2001**, *13*, 3306−3319.
(6) Stein, A.; Schroden, R. C. Colloidal Crystal Templating of Three-Dimensionally Ordered Macroporous Solids: Materials for Photonics and Beyond. *Curr. Opin. Solid State Mater. Sci.* **2001**, *5*, 553−564.
(7) Guliants, V. V.; Carreon, M. A.; Lin, Y. S. Ordered Mesoporous and Macroporous Inorganic Films and Membranes. *J. Membr. Sci.* **2004**, *235*, 53−72.
(8) Zeng, F.; Sun, Z. W.; Wang, C. Y.; Ren, B. Y.; Liu, X. X.; Tong, Z. Fabrication of Inverse Opal Via Ordered Highly Charged Colloidal Spheres. *Langmuir* **2002**, *18*, 9116−9120.
(9) Velev, O. D.; Jede, T. A.; Lobo, R. F.; Lenhoff, A. M. Microstructured Porous Silica Obtained Via Colloidal Crystal Templates. *Chem. Mater.* **1998**, *10*, 3597−3602.
(10) Hench, L. L.; West, J. K. The Sol Gel Process. *Chem. Rev.* **1990**, *90*, 33−72.

DOI: 10.1021/acsami.5b00656
ACS Appl. Mater. Interfaces 2015, 7, 6054−6061

(11) Ciriminna, R.; Fidalgo, A.; Pandarus, V.; Beland, F.; Ilharco, L. M.; Pagliaro, M. The Sol-Gel Route to Advanced Silica-Based Materials and Recent Applications. *Chem. Rev.* **2013**, *113*, 6592−6620.
(12) Fang, J. F.; Xuan, Y. M.; Li, Q. A. Preparation of Polystyrene Spheres in Different Particle Sizes and Assembly of the Ps Colloidal Crystals. *Sci. China-Technol. Sci.* **2010**, *53*, 3088−3093.
(13) Hatton, B.; Mishchenko, L.; Davis, S.; Sandhage, K. H.; Aizenberg, J. Assembly of Large-Area, Highly Ordered, Crack-Free Inverse Opal Films. *Proc. Natl. Acad. Sci. U. S. A.* **2010**, *107*, 10354−10359.
(14) Velev, O. D.; Lenhoff, A. M. Colloidal Crystals as Templates for Porous Materials. *Curr. Opin. Colloid Interface Sci.* **2000**, *5*, 56−63.
(15) Vong, M. S. W.; Bazin, N.; Sermon, P. A. Chemical Modification of Silica Gels. *J. Sol-Gel Sci. Technol.* **1997**, *8*, 499−505.
(16) Sun, Z. K.; Deng, Y. H.; Wei, J.; Gu, D.; Tu, B.; Zhao, D. Y. Hierarchically Ordered Macro-/Mesoporous Silica Monolith: Tuning Macropore Entrance Size for Size-Selective Adsorption of Proteins. *Chem. Mater.* **2011**, *23*, 2176−2184.
(17) Gornowich, D. B.; Blanchard, G. J. Enhancement of Enzyme Activity by Confinement in an Inverse Opal Structure. *J. Phys. Chem. C* **2012**, *116*, 12165−12171.
(18) Wen, J. Y.; Wilkes, G. L. Organic/Inorganic Hybrid Network Materials by the Sol-Gel Approach. *Chem. Mater.* **1996**, *8*, 1667−1681.
(19) Jung, H. Y.; Gupta, R. K.; Seo, D. W.; Kim, Y. H.; Whang, C. M. Preparation and Characterization of Hybrid Silica-Poly(Ethylene Glycol) Sonogel. *Bull. Korean Chem. Soc.* **2002**, *23*, 884−890.
(20) Linegar, K. L.; Adeniran, A. E.; Kostko, A. F.; Anisimov, M. A. Hydrodynamic Radius of Polyethylene Glycol in Solution Obtained by Dynamic Light Scattering. *Colloid J.* **2010**, *72*, 279−281.
(21) Jung, H. Y.; Gupta, R. K.; Oh, E. O.; Kim, Y. H.; Whang, C. M. Vibrational Spectroscopic Studies of Sol-Gel Derived Physical and Chemical Bonded Ormosils. *J. Non-Cryst. Solids* **2005**, *351*, 372−379.
(22) Griffith, G. W. Quantitation of Silanol in Silicones by Ftir Spectroscopy. *Ind. Eng. Chem. Prod. Res. Dev. Rev.* **1984**, *23*, 590−593.
(23) Grandi, S.; Magistris, A.; Mustarelli, P.; Quartarone, E.; Tomasi, C.; Meda, L. Synthesis and Characterization of SiO2-PEG Hybrid Materials. *J. Non-Cryst. Solids* **2006**, *352*, 273−280.
(24) Yoldas, B. E. Hydrolysis of Titanium Alkoxide and Effects of Hydrolytic Polycondensation Parameters. *J. Mater. Sci.* **1986**, *21*, 1087−1092.
(25) Blanco, A.; Chomski, E.; Grabtchak, S.; Ibisate, M.; John, S.; Leonard, S. W.; Lopez, C.; Meseguer, F.; Miguez, H.; Mondia, J. P.; Ozin, G. A.; Toader, O.; van Driel, H. M. Large-Scale Synthesis of a Silicon Photonic Crystal with a Complete Three-Dimensional Bandgap near 1.5 Micrometres. *Nature* **2000**, *405*, 437−440.
(26) Li, Y.; Piret, F.; Leonard, T.; Su, B. L. Rutile TiO2 Inverse Opal with Photonic Bandgap in the UV-Visible Range. *J. Colloid Interface Sci.* **2010**, *348*, 43−48.
(27) Rengarajan, R.; Mittleman, D.; Rich, C.; Colvin, V. Effect of Disorder on the Optical Properties of Colloidal Crystals. *Phys. Rev. E* **2005**, *71*.
(28) Takahashi, R.; Nakanishi, K.; Soga, N. Aggregation Behavior of Alkoxide-Derived Silica in Sol-Gel Process in Presence of Poly-(Ethylene Oxide). *J. Sol-Gel Sci. Technol.* **2000**, *17*, 7−18.
(29) Surivet, F.; Lam, T. M.; Pascault, J. P.; Pham, Q. T. Organic Inorganic Hybrid Materials 0.1. Hydrolysis and Condensation Mechanisms Involved in Alkoxysilane-Terminated Macromonomers. *Macromolecules* **1992**, *25*, 4309−4320.
(30) Huang, H.-H.; Wilkes, G. Structure-Property Behavior of New Hybrid Materials Incorporating Oligomeric Poly(Tetramethylene Oxide) with Inorganic Silicates by a Sol-Gel Process. *Polym. Bull.* **1987**, *18*, 455−462.

DOI: 10.1021/acsami.5b00656
ACS Appl. Mater. Interfaces 2015, 7, 6054−6061